NASA TN D-433

TECHNICAL NOTE

D-433

LOW-SPEED MEASUREMENTS OF STATIC AND OSCILLATORY LATERAL STABILITY DERIVATIVES OF A 1/5-SCALE MODEL OF A JET-POWERED VERTICAL-ATTITUDE VTOL RESEARCH AIRPLANE

By Robert E. Shanks and Charles C. Smith, Jr.

Langley Research Center
Langley Field, Va.

NATIONAL AERONAUTICS AND SPACE ADMINISTRATION
WASHINGTON

September 1960

NATIONAL AERONAUTICS AND SPACE ADMINISTRATION

TECHNICAL NOTE D-433

LOW-SPEED MEASUREMENTS OF STATIC AND OSCILLATORY LATERAL STABILITY DERIVATIVES OF A 1/5-SCALE MODEL OF A JET-POWERED VERTICAL-ATTITUDE VTOL RESEARCH AIRPLANE

By Robert E. Shanks and Charles C. Smith, Jr.

SUMMARY

An investigation has been made in the Langley free-flight tunnel to determine the low-speed static lateral stability characteristics and the rolling, yawing, and sideslipping dynamic stability derivatives of a 1/5-scale model of a jet-powered vertical-attitude VTOL research airplane. The results of this investigation are presented herein without analysis.

INTRODUCTION

An investigation has been made to determine the low-speed static lateral stability characteristics and the rolling, yawing, and sideslipping dynamic stability derivatives of a 1/5-scale model of a jet-powered vertical-attitude VTOL research airplane. The model used in this investigation was the flying model used previously in the flight-test investigation discussed in reference 1. The airplane has a modified triangular wing with a modified triangular vertical tail mounted on top of the wing and has no horizontal tail. A small vertical tail was also mounted on each wing tip to help improve the directional stability at low angles of attack. Take-offs and landings with the airplane in a vertical attitude are made from a horizontal wire with a special hook-on attachment on the nose of the airplane. For convenience, however, the airplane also had a tricycle landing gear to permit conventional take-offs from and landings on the ground so that the initial transitions could be performed at a safe altitude.

The investigation included rolling, yawing, and sideslipping oscillation tests over an angle-of-attack range from 0° to 90° with 0° deflection of all controls. The reduced-frequency parameter was varied from 0.05 to 0.23 in the rolling, yawing, and sideslipping oscillation tests.

DEFINITIONS OF TERMS AND SYMBOLS

All velocities, forces, and moments, with the exception of lift and drag, were measured with respect to the body-axis system originating at the reference center-of-gravity position located at 30.4 percent mean aerodynamic chord. Lift and drag were measured with respect to the wind-axis system. (See fig. 1.) The term "in-phase derivative" used herein refers to any one of the stability derivatives which are based on the forces or moments in phase with the angle of roll, yaw, or sideslip produced in the oscillatory tests. The term "out-of-phase derivative" refers to any one of the stability derivatives which are based on the forces or moments 90° out of phase with the angle of roll, yaw, or sideslip. The derivatives measured in the investigation are summarized in table I. All measurements are reduced to standard coefficient form and are presented in terms of the following symbols:

L
6
4
0

X,Y,Z	body reference axes
S	wing area, sq ft
b	wing span, ft
$\bar{c}$	mean aerodynamic chord, ft
V	free-stream velocity, ft/sec
q	free-stream dynamic pressure, lb/sq ft
$\omega = 2\pi f$,	radians/sec
f	frequency of oscillation, cps
k	reduced-frequency parameter, $\omega b/2V$
α	angle of attack, deg
β	angle of sideslip, deg or radians
r	yawing velocity, radians/sec
p	rolling velocity, radians/sec

t time, sec

$\dot{\beta} = \frac{d\beta}{dt}$

$\dot{r} = \frac{dr}{dt}$

$\dot{p} = \frac{dp}{dt}$

L
6
4
0

F_L lift, lb

F_D drag, lb

F_Y side force, lb

M_Y pitching moment, ft-lb

M_X rolling moment, ft-lb

M_Z yawing moment, ft-lb

C_m pitching-moment coefficient, $\frac{M_Y}{qS\bar{c}}$

C_l rolling-moment coefficient, $\frac{M_X}{qSb}$

C_n yawing-moment coefficient, $\frac{M_Z}{qSb}$

$C_{l_\beta} = \frac{\partial C_l}{\partial \beta}$ per radian

$C_{n_\beta} = \frac{\partial C_n}{\partial \beta}$ per radian

$C_{Y_\beta} = \frac{\partial C_Y}{\partial \beta}$ per radian

C_L lift coefficient, $\frac{F_L}{qS}$

C_D drag coefficient, $\frac{F_D}{qS}$

C_Y side-force coefficient, $\frac{F_Y}{qS}$

ϕ angle of roll, radians

ψ angle of yaw, radians

$$C_{l_r} = \frac{\partial C_l}{\partial \frac{rb}{2V}} \qquad C_{n_r} = \frac{\partial C_n}{\partial \frac{rb}{2V}} \qquad C_{Y_r} = \frac{\partial C_Y}{\partial \frac{rb}{2V}}$$

$$C_{l_p} = \frac{\partial C_l}{\partial \frac{pb}{2V}} \qquad C_{n_p} = \frac{\partial C_n}{\partial \frac{pb}{2V}} \qquad C_{Y_p} = \frac{\partial C_Y}{\partial \frac{pb}{2V}}$$

$$C_{l_{\dot\beta}} = \frac{\partial C_l}{\partial \frac{\dot\beta b}{2V}} \qquad C_{n_{\dot\beta}} = \frac{\partial C_n}{\partial \frac{\dot\beta b}{2V}} \qquad C_{Y_{\dot\beta}} = \frac{\partial C_Y}{\partial \frac{\dot\beta b}{2V}}$$

$$C_{l_{\dot r}} = \frac{\partial C_l}{\partial \frac{\dot r b^2}{4V^2}} \qquad C_{n_{\dot r}} = \frac{\partial C_n}{\partial \frac{\dot r b^2}{4V^2}} \qquad C_{Y_{\dot r}} = \frac{\partial C_Y}{\partial \frac{\dot r b^2}{4V^2}}$$

$$C_{l_{\dot p}} = \frac{\partial C_l}{\partial \frac{\dot p b^2}{4V^2}} \qquad C_{n_{\dot p}} = \frac{\partial C_n}{\partial \frac{\dot p b^2}{4V^2}} \qquad C_{Y_{\dot p}} = \frac{\partial C_Y}{\partial \frac{\dot p b^2}{4V^2}}$$

APPARATUS AND MODEL

Conventional static force tests were conducted in the Langley free-flight tunnel with the model sting mounted, and the forces and moments were measured about the body axes by means of a three-component internal strain-gage balance. The rotary and linear oscillation tests were also conducted in the Langley free-flight tunnel. Detailed descriptions of the apparatus and methods used in deriving the data are given in reference 2. A three-view drawing of the model is shown in figure 2, and the dimensional characteristics are given in table II. For all the tests the engine air inlets and exit were open to permit air flow through the model.

L
6
4
0

TESTS

The static force tests were made over an angle-of-attack range from 0° to 80° with all controls at 0° deflection. For angles of attack from 0° to 50° the sideslip angles were obtained by yawing the model about the tunnel vertical reference axis and for angles of attack from 40° to 80° the sideslip angles were obtained by rolling the model about its x body axis. The oscillation tests were made over an angle-of-attack range from 0° to 90° with all controls at 0° deflection. The reduced-frequency parameter k was varied from 0.05 to 0.23. An oscillation amplitude of $\pm 10^\circ$ was used in all the rolling and yawing tests, whereas the amplitude in the sideslipping tests was ± 0.417 foot or $\pm 0.62^\circ$ to $\pm 2.85^\circ$.

The static and the oscillatory tests were made at a dynamic pressure of 4.11 pounds per square foot, which corresponds to an airspeed of about 60 feet per second at standard sea-level conditions and to a test Reynolds number of 928,000 based on the mean aerodynamic chord of 2.425 feet.

PRESENTATION OF RESULTS

The results of this investigation are presented herein without discussion. The lift, drag, and pitching-moment characteristics of the model with zero deflection of all controls are presented in figure 3 in order that the reader may interpret the lateral stability data of the subsequent figures in terms of lift coefficient and airspeed if he so desires. The static lateral stability characteristics of the model are presented in figures 4 and 5. The variations of the rolling and yawing oscillation derivatives with the reduced-frequency parameter are shown in figures 6 and 7, respectively, for each of the angles of attack tested. The out-of-phase and in-phase derivatives are summarized in figures 8 and 9, respectively, in terms of the variation of the derivatives with angle of attack for constant values of the reduced-frequency parameter. In order

to afford a comparison between the data obtained from the in-phase oscillation tests and the static data, the data of figure 5 multiplied by the appropriate trigonometric function ($\sin \alpha$ for the rolling derivatives and $\cos \alpha$ for the yawing derivatives) have also been presented in figure 9.

In order to obtain the most reliable results in lateral stability calculations, derivatives such as C_{n_r} and $C_{n_{\dot{\beta}}}$ should be used independently in the equations rather than in the combination form $C_{n_r} - C_{n_{\dot{\beta}}} \cos \alpha$. Since $\dot{\beta}$ derivatives were measured in this investigation, it is possible to break up the combination derivatives into their component parts. The values of C_{n_p}, C_{l_p}, C_{n_r}, and C_{l_r} presented in figure 10 were therefore obtained by taking the difference between the $\dot{\beta}$ derivatives and the combination derivatives presented in figure 8.

L
6
4
0

CONCLUDING REMARKS

An investigation has been made to determine the low-speed static and dynamic stability characteristics and the rolling, yawing, and sideslipping dynamic stability derivatives of a 1/5-scale model of a jet-powered vertical-attitude VTOL research airplane. The results are presented without analysis in a form convenient for estimating the characteristics of similar configurations.

Langley Research Center,
National Aeronautics and Space Administration,
Langley Field, Va., August 14, 1959.

REFERENCES

1. Smith, Charles C., Jr.: Hovering and Transition Flight Tests of a 1/5-Scale Model of a Jet-Powered Vertical-Attitude VTOL Research Airplane. NASA MEMO 10-27-58L, 1958.

2. Hewes, Donald E.: Low-Subsonic Measurements of the Static and Oscillatory Lateral Stability Derivatives of a Sweptback-Wing Airplane Configuration at Angles of Attack From -10° to 90°. NASA MEMO 5-20-59L, 1959.

TABLE I

DERIVATIVES MEASURED IN OSCILLATORY TESTS

Derivatives	Rolling	Yawing	Sideslipping
In-phase	$C_{l_\beta} \sin \alpha - k^2 C_{l_{\dot{p}}}$ $C_{n_\beta} \sin \alpha - k^2 C_{n_{\dot{p}}}$ $C_{Y_\beta} \sin \alpha - k^2 C_{Y_{\dot{p}}}$	$C_{l_\beta} \cos \alpha + k^2 C_{l_{\dot{r}}}$ $C_{n_\beta} \cos \alpha + k^2 C_{n_{\dot{r}}}$ $C_{Y_\beta} \cos \alpha + k^2 C_{Y_{\dot{r}}}$	C_{l_β} C_{n_β} C_{Y_β}
Out-of-phase	$C_{l_p} + C_{l_{\dot{\beta}}} \sin \alpha$ $C_{n_p} + C_{n_{\dot{\beta}}} \sin \alpha$ $C_{Y_p} + C_{Y_{\dot{\beta}}} \sin \alpha$	$C_{l_r} - C_{l_{\dot{\beta}}} \cos \alpha$ $C_{n_r} - C_{n_{\dot{\beta}}} \cos \alpha$ $C_{Y_r} - C_{Y_{\dot{\beta}}} \cos \alpha$	$C_{l_{\dot{\beta}}}$ $C_{n_{\dot{\beta}}}$ $C_{Y_{\dot{\beta}}}$

TABLE II

GEOMETRIC CHARACTERISTICS OF MODEL

Wing (modified triangular plan form):	
Sweepback, deg	60
Airfoil section	NACA 65A008
Aspect ratio	1.97
Area, sq in.	1,094.4
Span, in.	46.4
Mean aerodynamic chord, in.	29.1
Moment arm of roll nozzles, in.	24.375
Incidence, deg	4
Dihedral, deg	0
Overall length of model, in.	56.25
Vertical tail (modified triangular plan form):	
Sweepback, deg	45
Airfoil section	NACA 65A012
Aspect ratio	1.76
Area, sq in.	270
Span, in.	22
Outboard fin:	
Airfoil section	NACA 65A011
Area, each, sq in.	23.4
Area, total, sq in.	46.8
Aspect ratio	3.57
Span, in.	9.14
Root chord, in.	7.02
Tip chord, in.	3.07

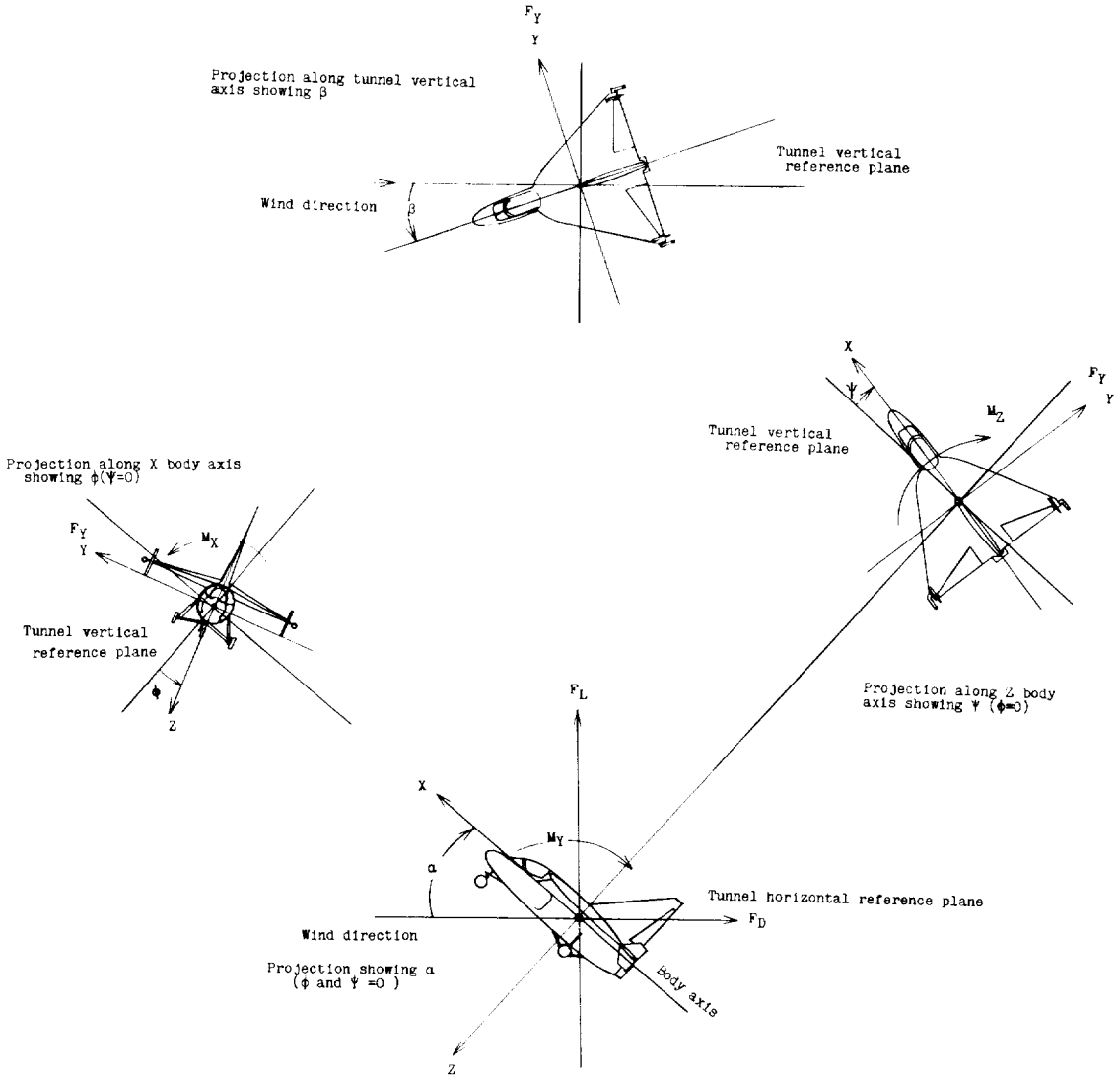

Figure 1.- Body system of axes. Arrows indicate positive directions of moments, forces, and angles. This system of axes is defined as an orthogonal system having the origin at the center of gravity, and the X-axis is in the plane of symmetry and alined with the longitudinal axis of the fuselage. The Z-axis is in the plane of symmetry and perpendicular to the X-axis, and the Y-axis is perpendicular to the plane of symmetry.

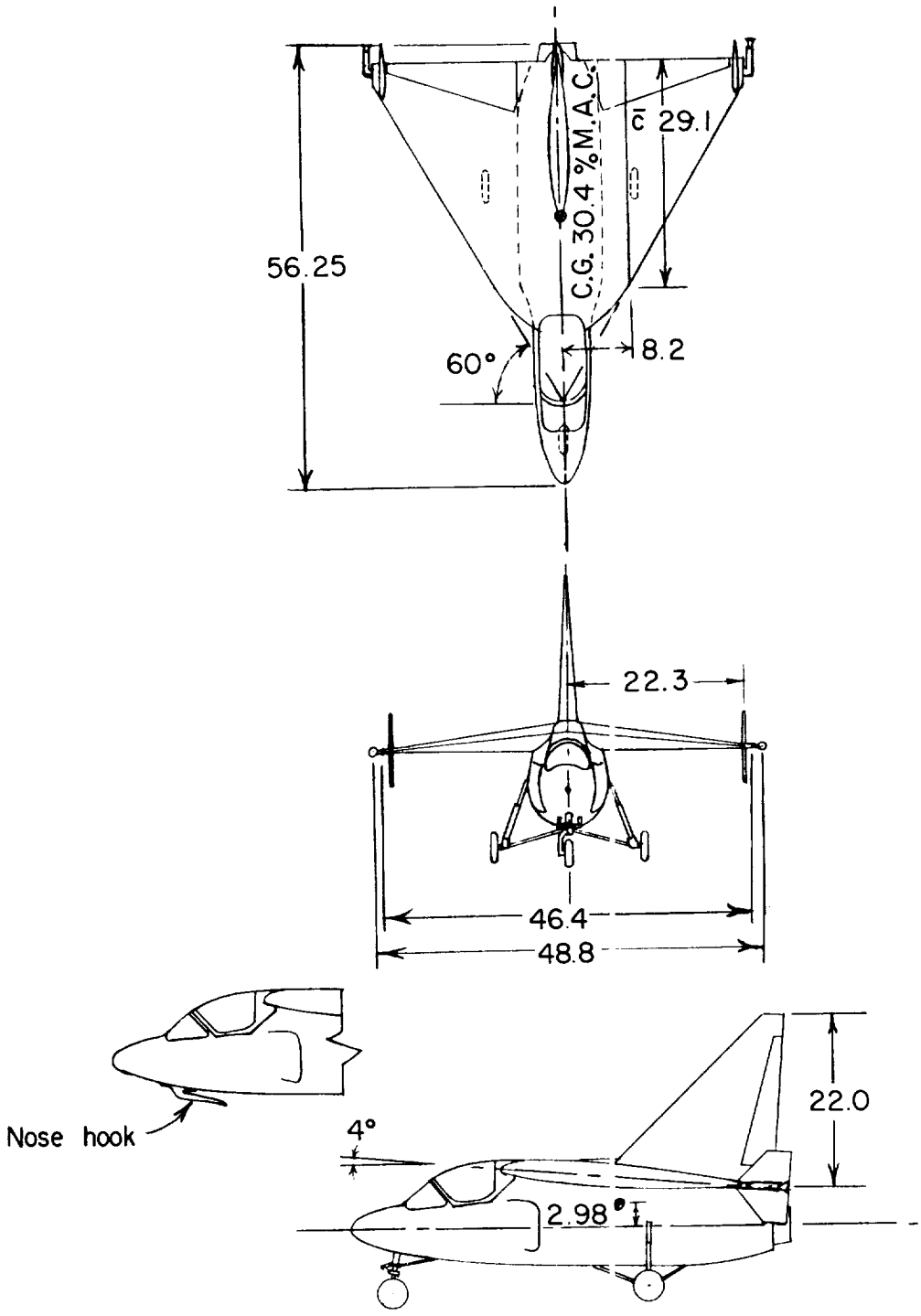

Figure 2.- Three-view sketch of the model used in the tests. All dimensions are in inches unless otherwise indicated.

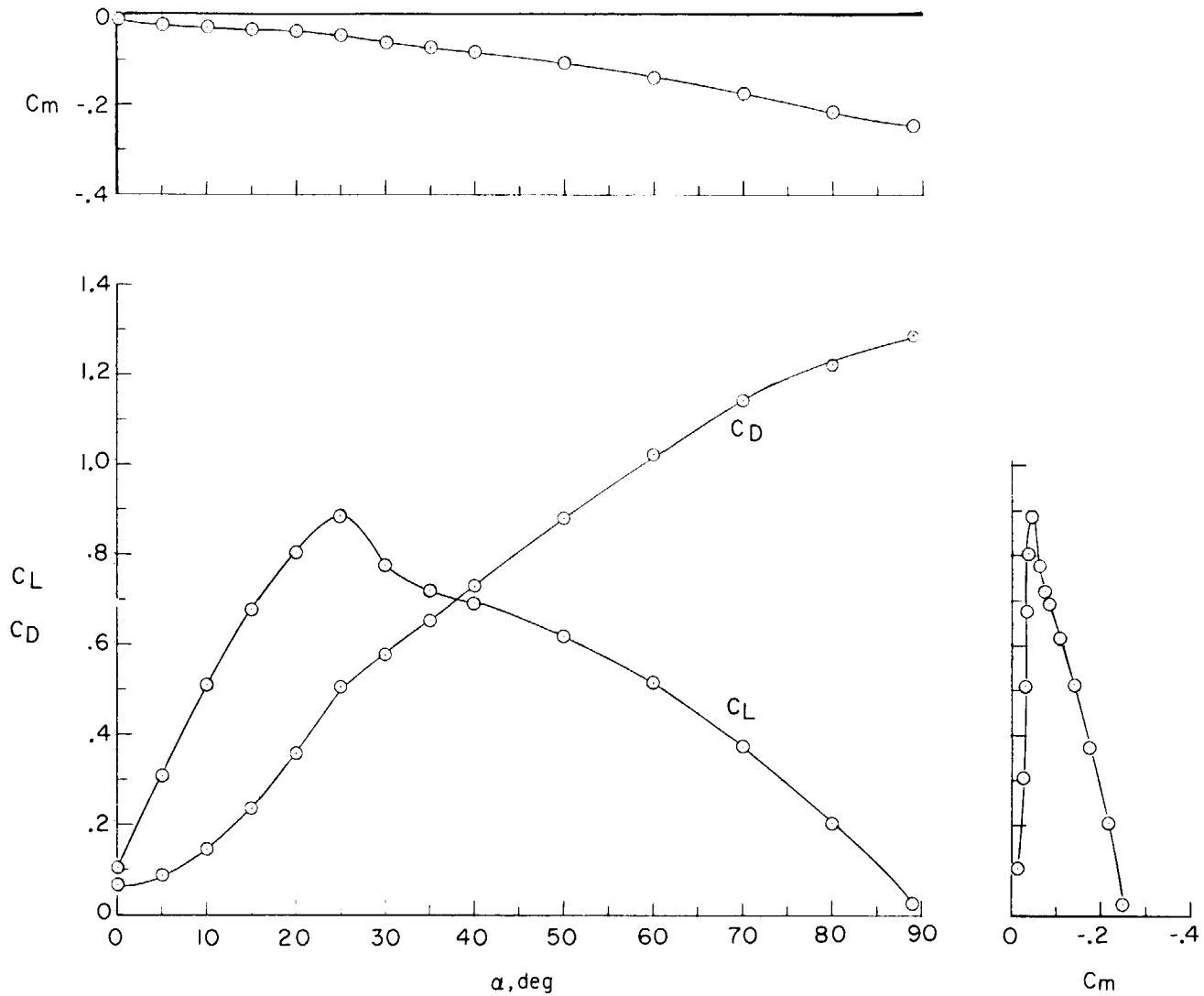

Figure 3.- Static longitudinal characteristics of the model. $\beta = 0^{\circ}$.

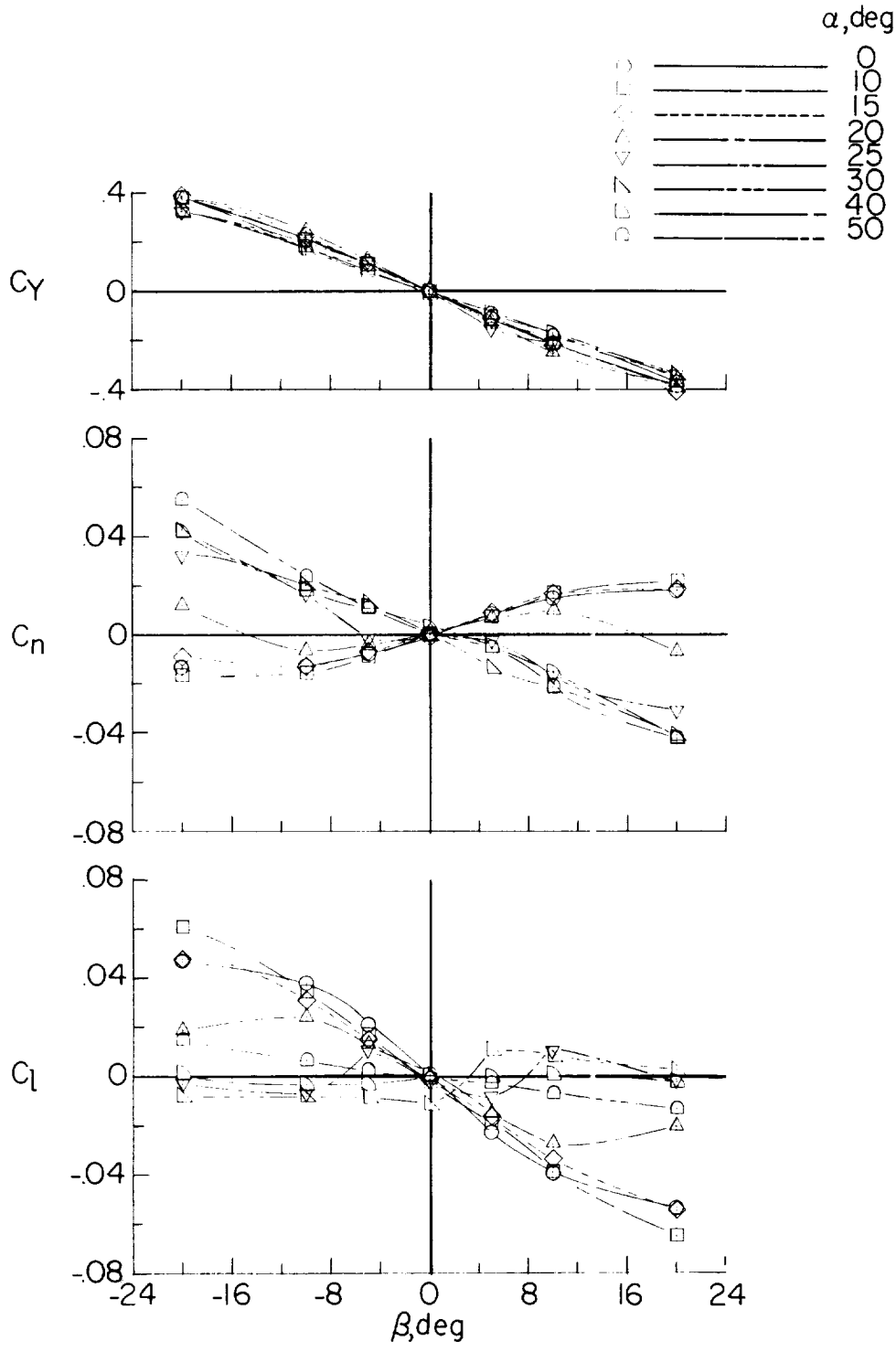

Figure 4.- Static lateral stability characteristics of model.

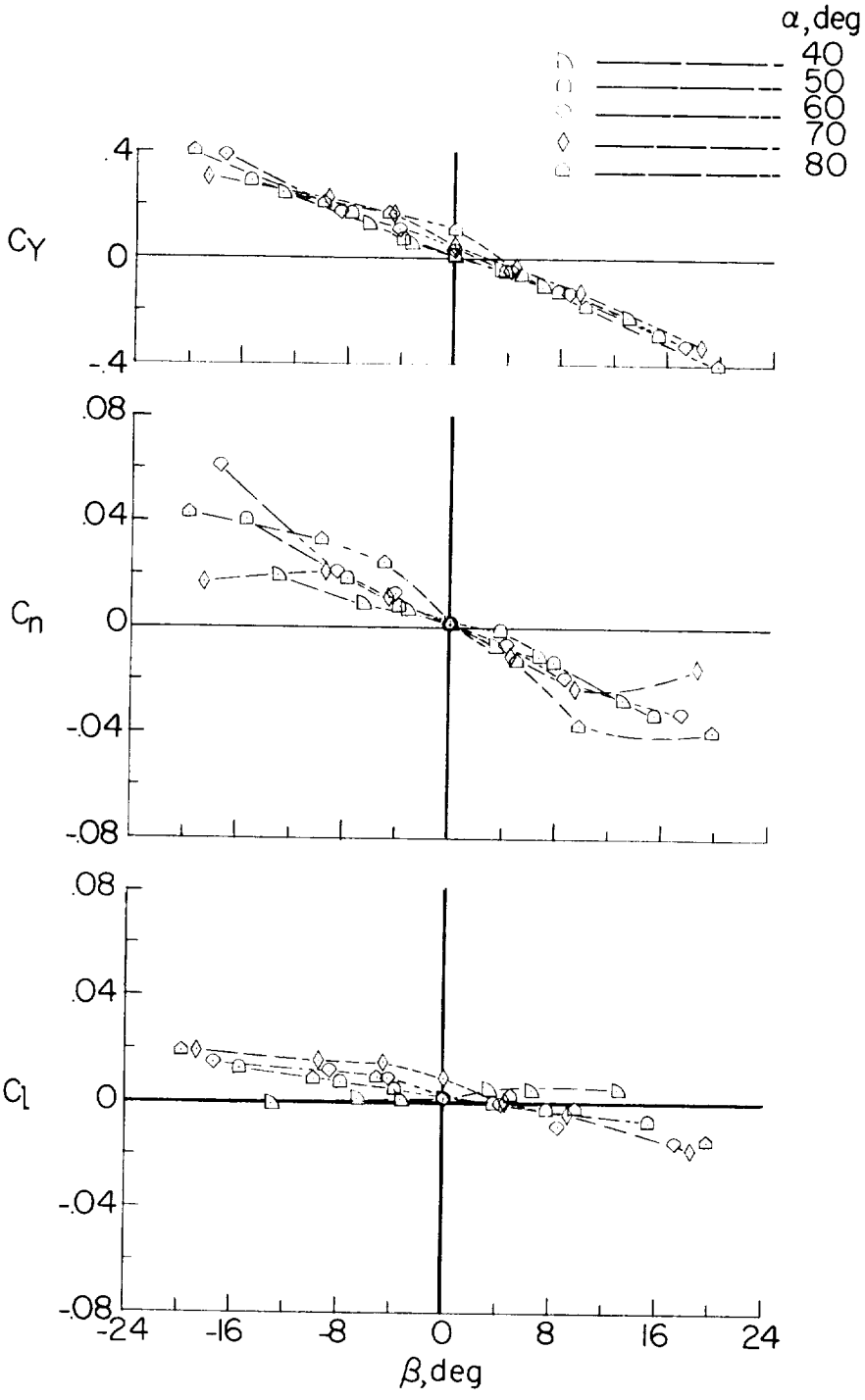

Figure 4.- Concluded.

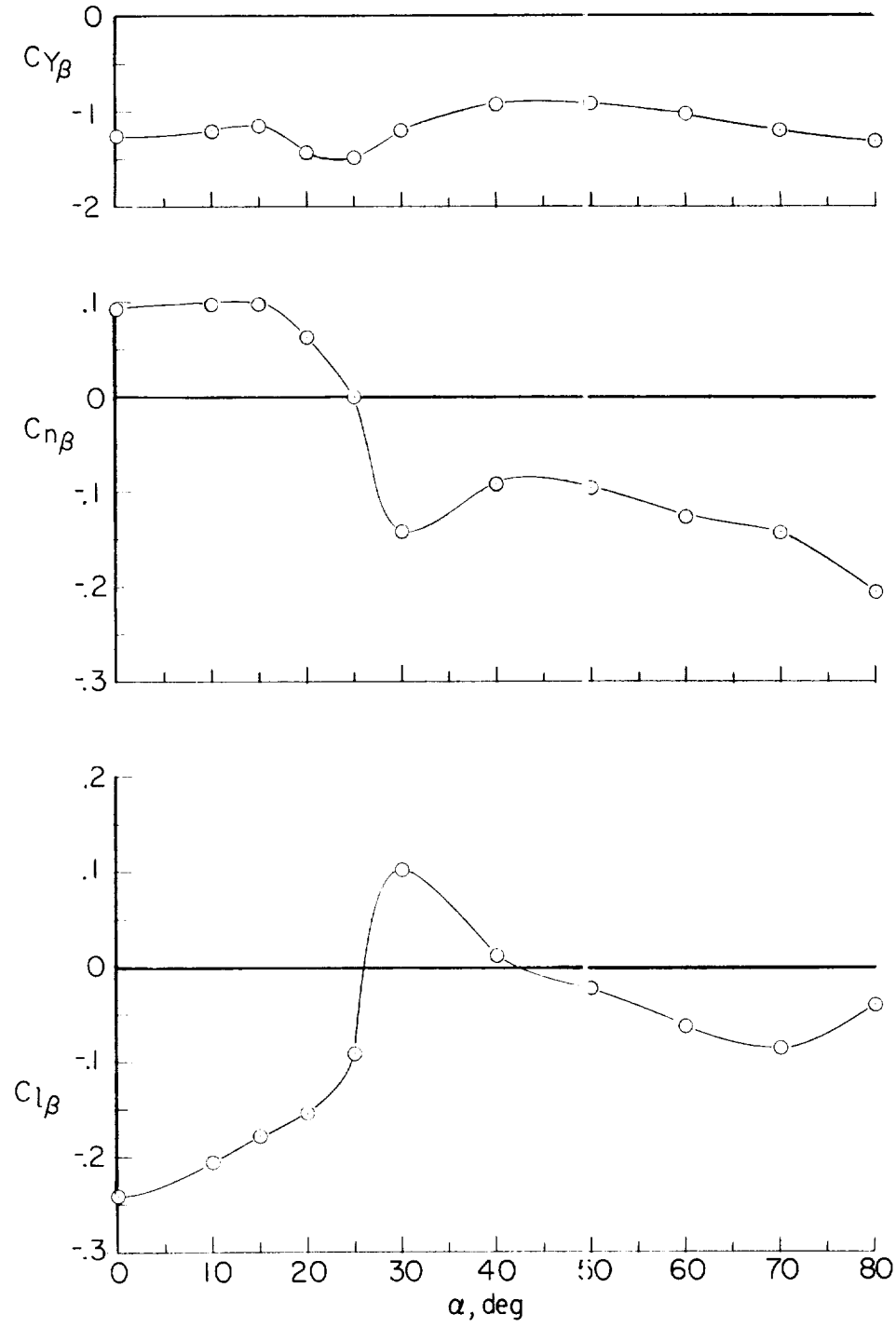

Figure 5.- Variation of static lateral stability derivatives with angle of attack. $\beta = \pm 5^\circ$.

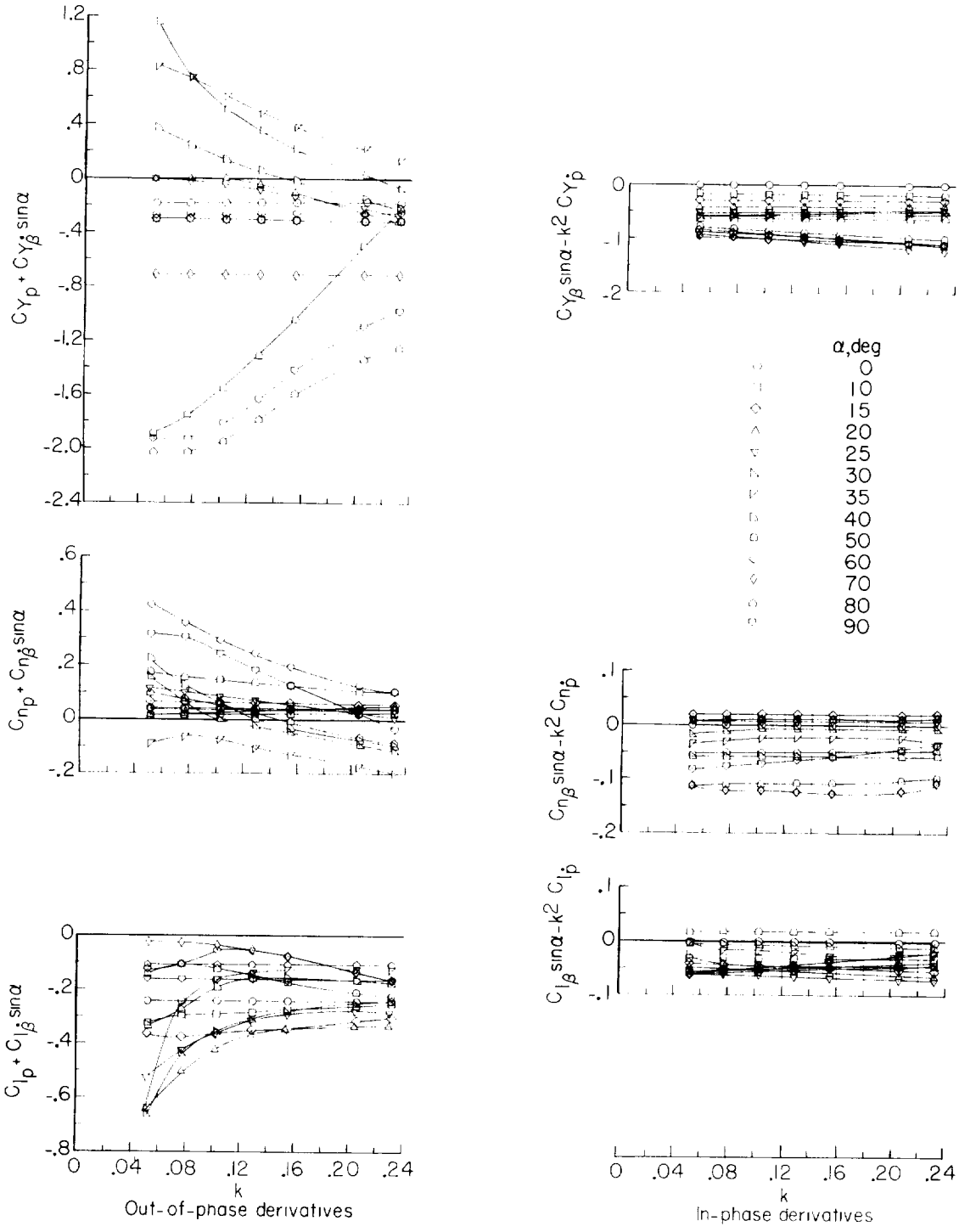

Figure 6.- Variation of rolling oscillation derivatives with reduced-frequency parameter.

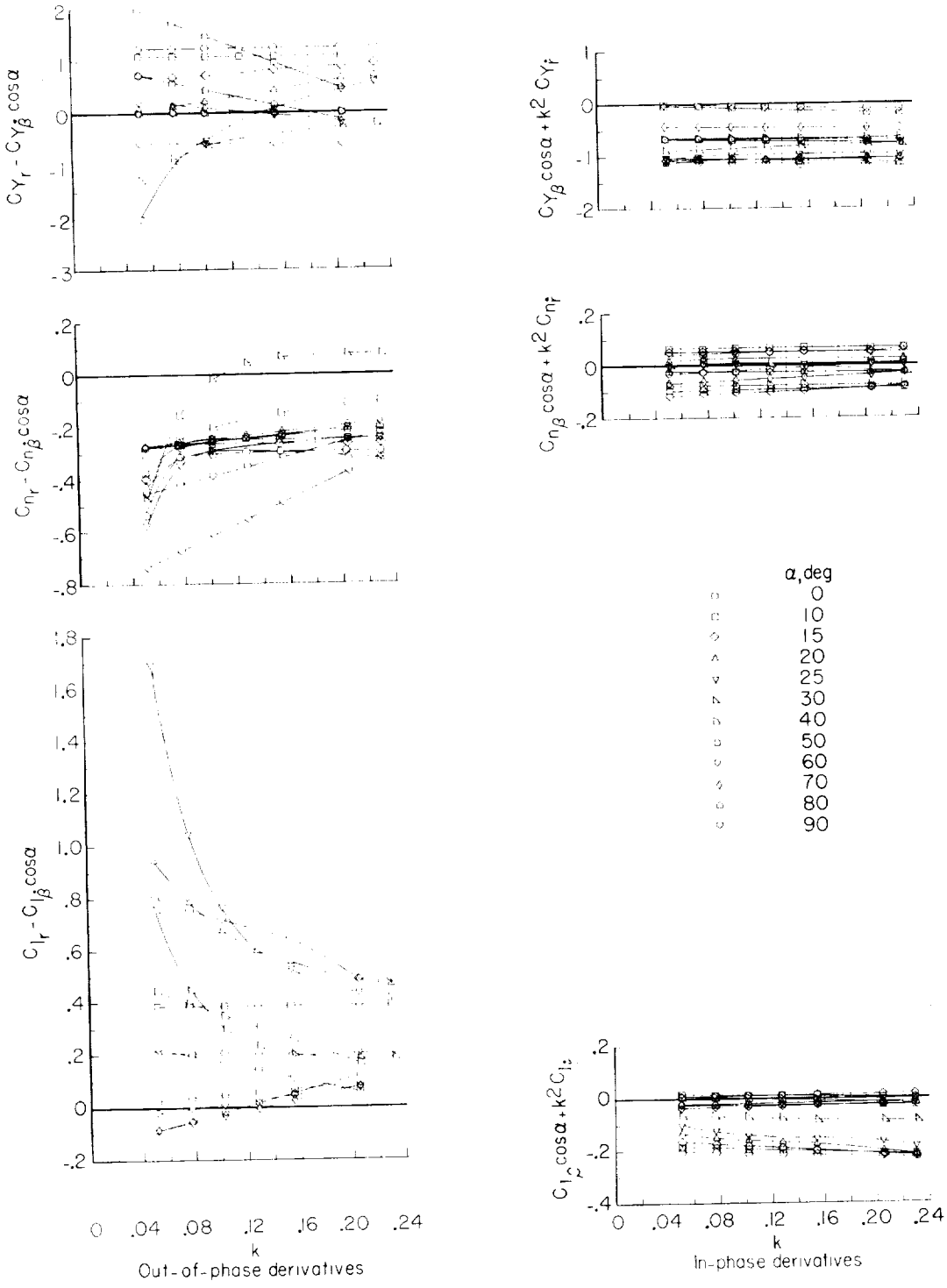

Figure 7.- Variation of yawing oscillation derivatives with reduced-frequency parameter.

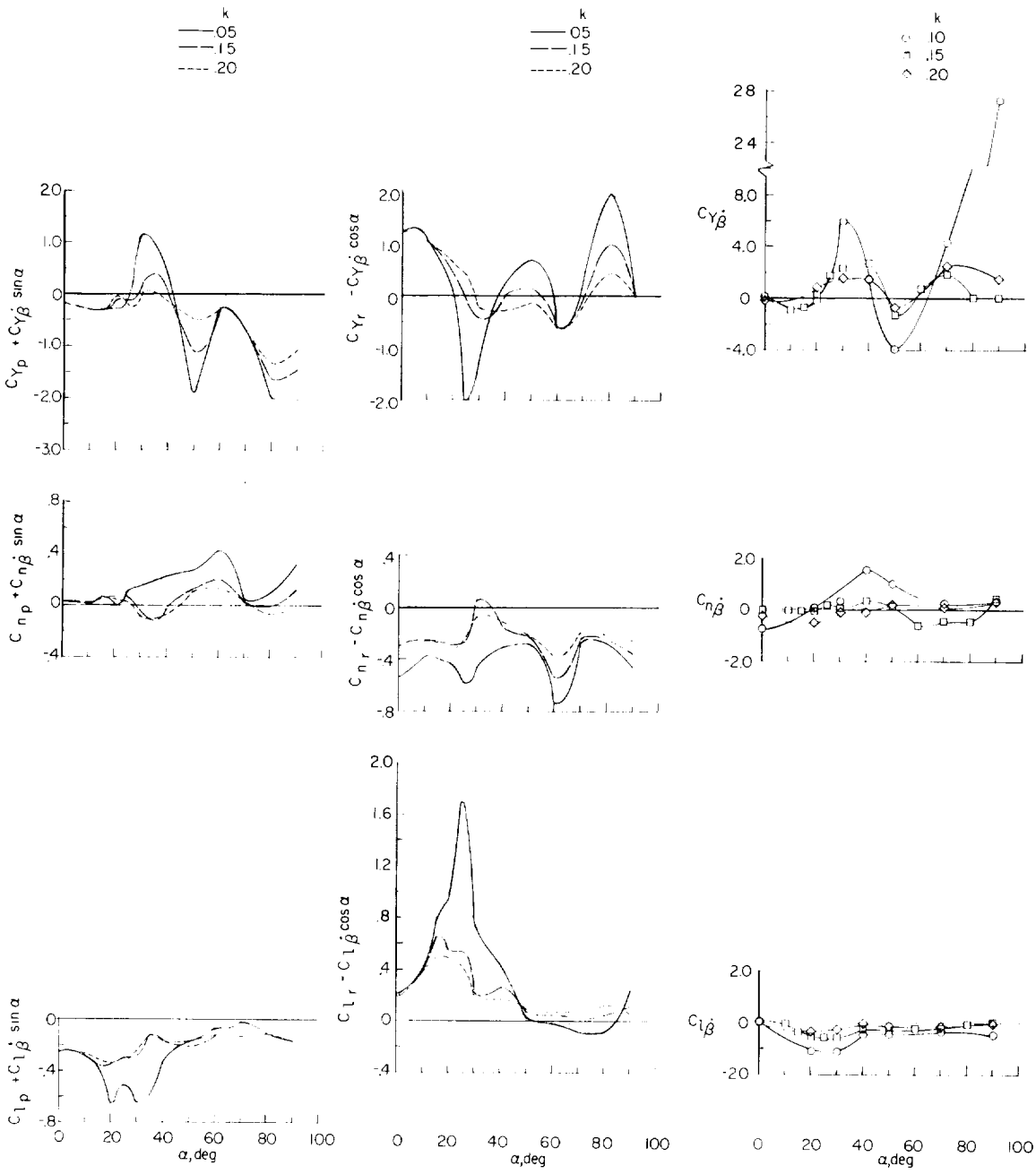

Figure 8.- Variation of out-of-phase derivatives with angle of attack.

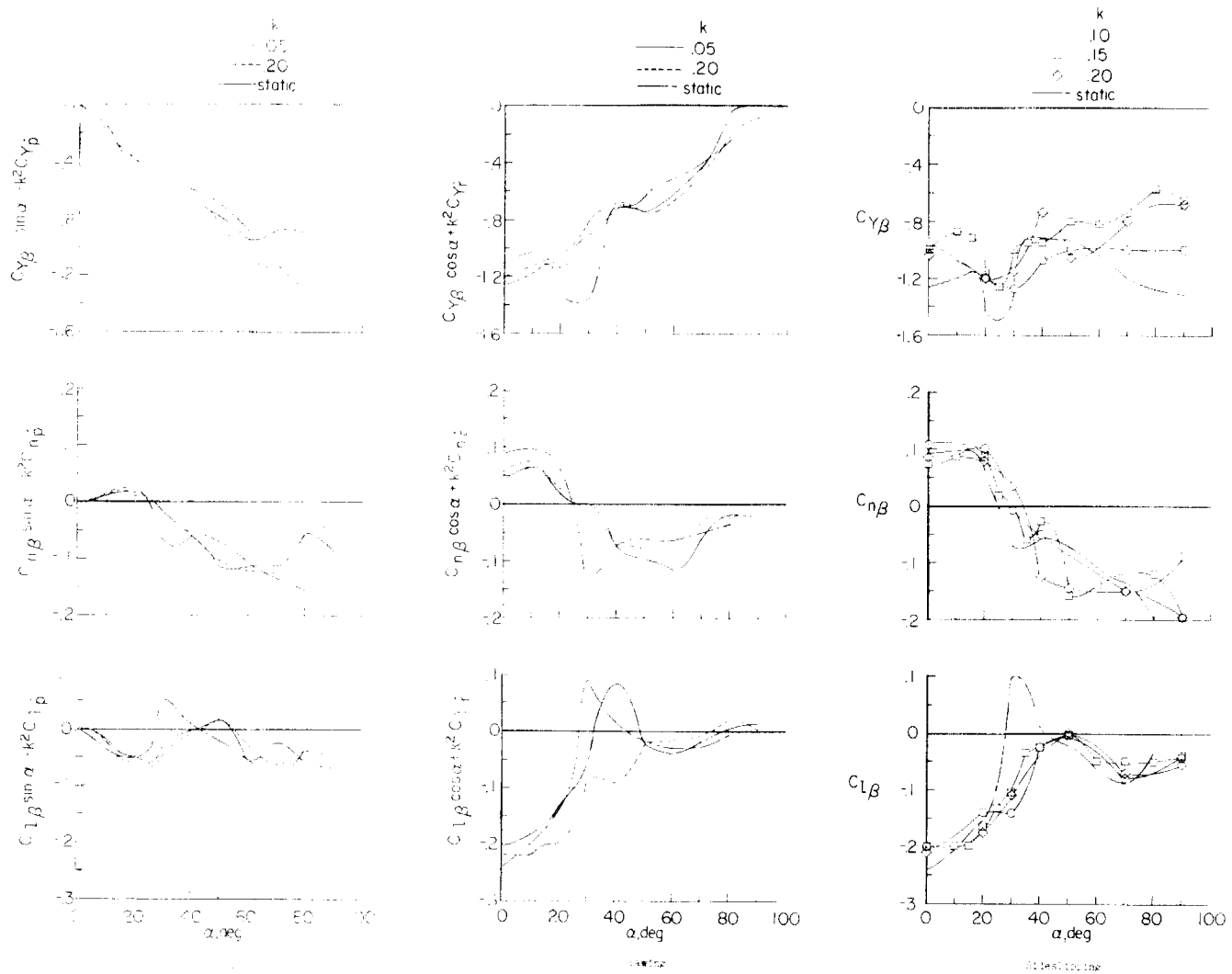

Figure 9.- Variation of in-phase derivatives with angle of attack.

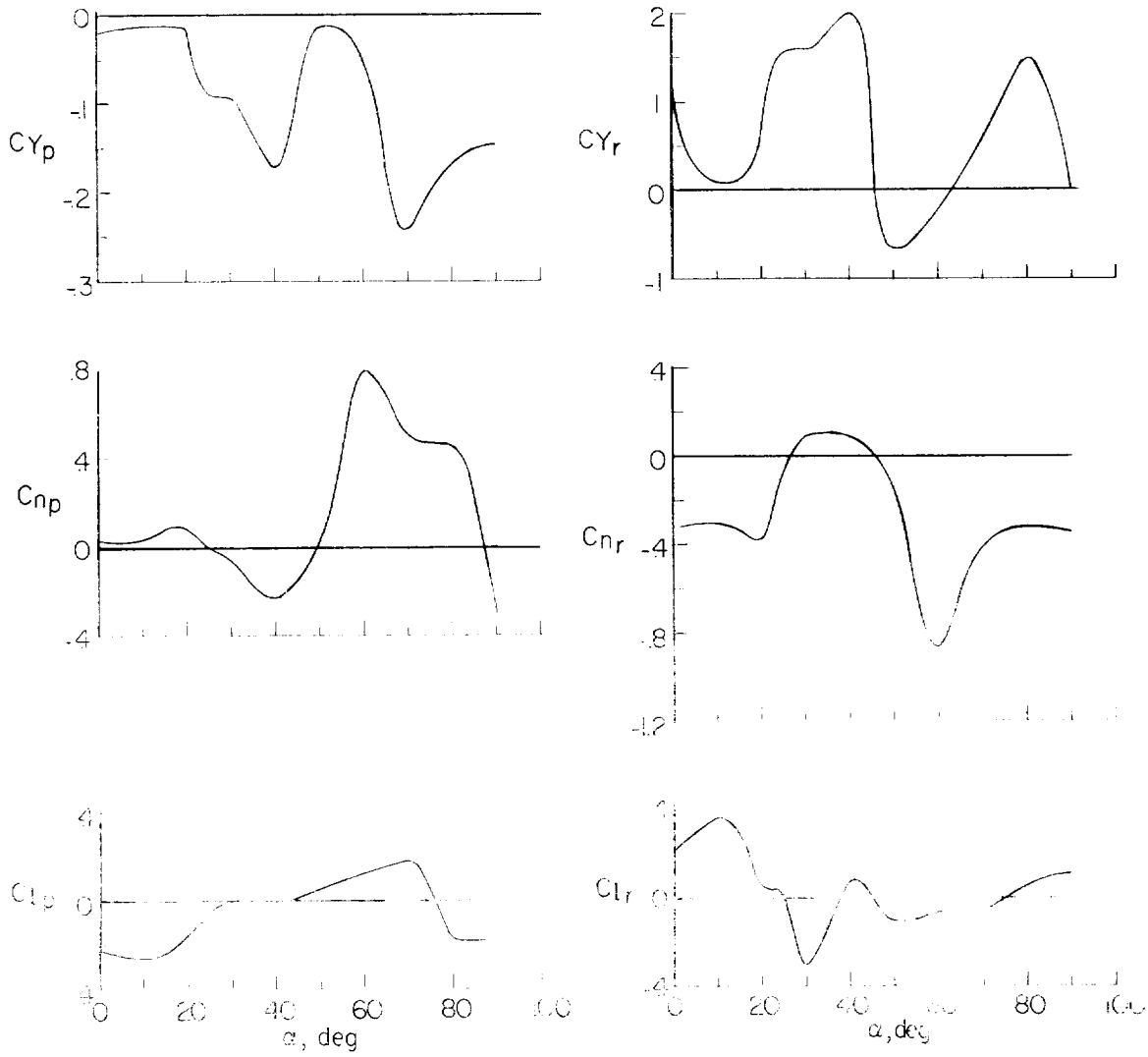

Figure 10.- Variation of rolling and yawing stability derivatives with angle of attack. Determined from data for k = 0.1 in figure 8